Fuel 276 (2020) 118099

Contents lists available at ScienceDirect

Fuel

journal homepage: www.elsevier.com/locate/fuel

Full Length Article

Insight into the enhanced performance of toluene removal from simulated flue gas over Mn-Cu oxides modified activated coke

Yindi Zhang[a,b], Caiting Li[a,b,*], Youcai Zhu[a,b], Xueyu Du[a,b], Yue Lyu[a,b], Shanhong Li[a,b], Yunbo Zhai[a,b]

[a] College of Environmental Science and Engineering, Hunan University, Changsha 410082, PR China
[b] Key Laboratory of Environmental Biology and Pollution Control (Hunan University), Ministry of Education, Changsha 410082, PR China

GRAPHIC ABSTRACT

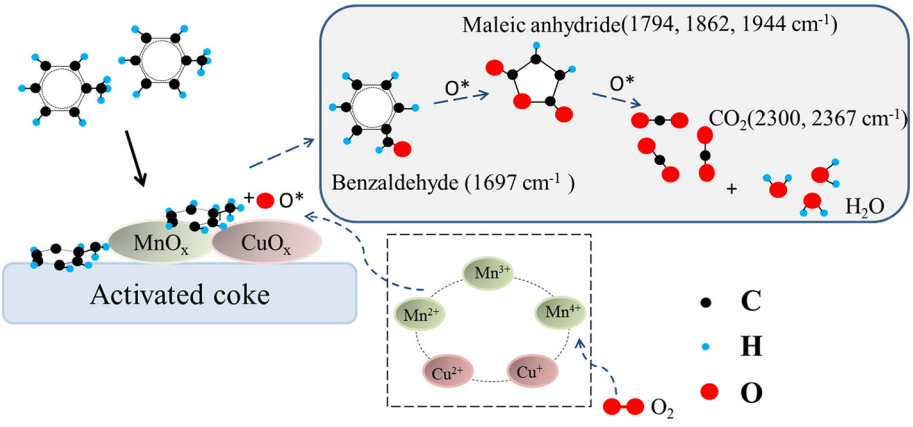

ARTICLE INFO

Keywords:
Toluene
Activated coke
Mn-Cu oxides
Simulated flue gas
Catalytic removal

ABSTRACT

A series of bimetallic oxides of manganese and copper with different loading of copper loaded on activated coke (Mn_xCu_y/AC) were synthesized by ultrasound-assisted equivalent volume impregnation method for toluene oxidation in simulated flue gas at 150–300 °C. The physicochemical properties of samples have been investigated by means of XRD, SEM, BET, XPS, H_2-TPR and DRIFT. Mn_6Cu_5/AC exhibited the enhanced toluene removal efficiency (99.38%) at 270 °C, as well as satisfactory reusability and durability. The excellent activity of Mn_6Cu_5/AC was connected with the highly uniform distribution of active components and the larger specific surface area, which confirmed the synergistic interaction between MnO_x and CuO_x, thus leading to the stronger reducibility and the good oxygen mobility. In addition, SO_2 and NO played a hindering role due to the competitive adsorption of active sites in pure N_2, whereas the negative effect would be reduced by the introduction of O_2. Besides, the influence of H_2O on toluene removal was complex. Moreover, the reaction process obtained from DRIFT indicated that toluene can be rapidly adsorbed and activated to form the benzaldehyde and maleic anhydride species on Mn_6Cu_5/AC, and finally be further oxidized into CO_2 and H_2O. Finally, the mechanism of toluene oxidation over Mn_6Cu_5/AC was proposed.

* Corresponding author at: College of Environmental Science and Engineering, Hunan University, Changsha 410082, PR China.
E-mail address: ctli@hnu.edu.cn (C. Li).

https://doi.org/10.1016/j.fuel.2020.118099
Received 22 November 2019; Received in revised form 23 April 2020; Accepted 13 May 2020

1. Introduction

In the last decades, VOCs pollution from anthropogenic sources has become an increasingly alarming problem due to its contributor to the wealth atmospheric pollution, important precursors of ozone and $PM_{2.5}$ and cooperating with NO_x to contribute to the formation of photochemical smog and haze [1–4]. Moreover, as a representative VOC, toluene is widely considered as a great threat to human health [5–9]. For example, long-term exposure to parts per million (ppm) toluene-containing atmospheres may cause serious chronic diseases and lead to "mutagenic-teratogenic-carcinogenic" effect [10,11]. Therefore, more increasingly strict legislations are enacted for stringent emission of VOCs [2]. For instance, toluene has been considered as one of the 189 hazardous air pollutants listed in the 1990 Clean Air Act Amendment (CAAA90) proposed by the US Environmental Agency [12]. Hence, developing effective technologies for toluene removal are of great significance and central urgency.

Numerous research initiatives around the world have been dedicated to efficient technologies for toluene removal to meet the stringent environmental regulations, such as incineration, condensation [13], adsorption [14], absorption, plasma technology [15] and catalytic oxidation, etc. Among the strategies mentioned above [16], with the minimization of the formed toxic by-products, catalytic oxidation is considered as the most effective and economically feasible method [17,18]. Nevertheless, because of the dependence of this method on catalyst, the search for catalytic materials with high activity, low cost and high tolerability are of great significance.

Up to now, two main groups of catalytic materials are usually employed for the removal of toluene: (i) supported or unsupported noble metal catalysts (mainly Pt and Pd), and (ii) transition metal oxide-based catalysts. Although noble metal catalysts are characterized by durable and high activity at relatively low temperatures, their disadvantages of high cost and distinct deficiency of sensitive to poisoning still restrict their practical application [19,20]. Alternatively, transition metal oxides due to the advantages of lower cost, better resistant to poisoning and higher thermal stability received extensive attention [21–25]. According to the previous studies [26], manganese oxide own polymorphism and polyvalence derived from its electronic structure, which is favorable to the formation of labile lattice oxygen and the enhancement of storing oxygen capacity in the crystalline structure. Hence, MnO_x has been widely considered as a promising active phase for toluene abatement [27]. However, the catalytic performances of single-oxide catalysts are still away from arrival the satisfied catalytic performance to pollutants with complex structure in terms of activity and stability. To overcome these limitations, a promising strategy which combines the advantages of improve surface area and catalytic activity by loading another component was proposed [22]. For example, Chen et al. [28] reported that CoCe/ACs exhibited more superior removal efficiencies of Hg^0 and HCHO than Co/ACs and Ce/ACs due to the enhanced active oxygen mobility. Chen et al. [24] demonstrated that Mn-Fe possess higher surface area, higher concentration of lattice defects and oxygen vacancies than that of the Mn oxides, resulting in higher catalytic activity. According to the literature [29], the large π bond in the aromatic ring of phenyl VOCs is easily complexed with Cu to be activated, it was also demonstrated that the loading of CuO_x could facilitate the formation of defective oxygen and stabilized manganese at higher oxidation state that are vital for the oxidation of VOCs. As a typical mixed metal oxide, Mn-Cu bimetallic oxides samples might inherit the high toluene removal performance of MnO_x and the affinity to large π bond of CuO_x simultaneously. Especially, there are already some examples of applications of Mn-Cu mixed oxide, such as the oxidation of CO, NO and VOCs [30–34].

However, metal oxides without support are inconvenient for industrial applications due to their small specific surface area and high production costs. As a consequence, the participation of support is essential. Recently, carbon-based supports have attracted considerable attention due to its low cost and unique pore structures [27]. Hereinto, activated coke (AC) is regarded as a promising support by virtue of superior mechanical strength to withstand abrasion and crushing in industrial applications [35–37]. In addition, the superior pore structure of AC could adsorb toluene more easily, which is benefit for the following oxidation [37]. Nevertheless, virgin AC presents poor toluene removal ability on account of the limited physicochemical property. In this respect, modifying AC with metal oxides have been reported to be an effective method to increase the adsorption and catalytic ability [27,36,38]. Metal oxides as active components can be attached and further interact with the support, allowing the prepared catalysts to achieve a larger specific surface area and also greatly influencing the properties of the supported catalysts [39]. Although the copper and manganese bimetal oxides have been studied to some extent, the studies of them loaded on AC is scarce.

The present work aimed to investigate the catalytic behavior of MnO_x and CuO_x deposited on AC for removal of toluene, with emphasis on four aspects: (i) the influence of manganese and/or copper loading and reaction temperatures on toluene removal performance; (ii) the physicochemical and structural properties of the samples characterized by SEM, BET, XRD, H_2-TPR and XPS; (iii) the influence of flue gas components (O_2, SO_2, NO and H_2O) on toluene removal and the reusability and durability of sample; (iv) the possible mechanism of toluene removal was reasonably deduced by DRIFTS. The objective of the work is to develop a catalyst with industrial application value for toluene removal and give an in-depth exploration in the relationship between the physicochemical properties and catalytic activity of samples.

2. Experimental section

2.1. Samples preparation

2.1.1. Preparation of activated coke as support

Prior to impregnation, cylindrical granule commercial AC (D = 5 mm and L = 8–10 mm, Alxa League Ke'xing Carbon industry, China) was washed with deionized water repeatedly and then dried in an electric blast oven at 105 °C for 12 h; subsequently, the AC that had been washed before was ground and sieved repeatedly in order to obtain the corresponding powders of 40–60 mesh, the resulting powders were employed as support.

2.1.2. Synthesis of samples

All the samples were prepared using the ultrasound-assisted equivalent volume impregnation method. The modified procedures were described as follows: the AC (40-60 mesh) was impregnated in a calculated amounts of 50 wt% $Mn(NO_3)_2$ solution or/and $Cu(NO_3)_2{\cdot}3H_2O$ solution, subsequently the mixture were exposed to an ultrasonic bath for 1 h and then maintained at 30 °C for 23 h. After impregnation for 24 h, the obtained powders were dried in a drying oven at 105 °C for 12 h and calcined in an electric tube furnace at 500 °C for 4 h under N_2 atmosphere. The final samples obtained were denoted as Mn_x/AC, Cu_y/AC or Mn_xCu_y/AC, where x and y represented the mass percent of element Mn and Cu on the samples, respectively. The value of x was set as 4, 6, 8 and the value of y was set as 1, 2, 3, 4, 5, 6.

2.2. Samples characterization

The actual content of metal doping over modified samples was characterized by an Inductively Coupled Plasma-Atomic Emission Spectrometry (ICP–AES, SPECTRO BLUE SOP, Germany). The sample powders were structurally characterized by X-ray diffraction (XRD) patterns recorded using a Riguku D/Max 2550 powder diffractometer (Rigaku, Japan). Scanning electron microscopy (SEM) micrographs and Energy dispersive X-ray analyzer (EDX) were collected on a TESCAN

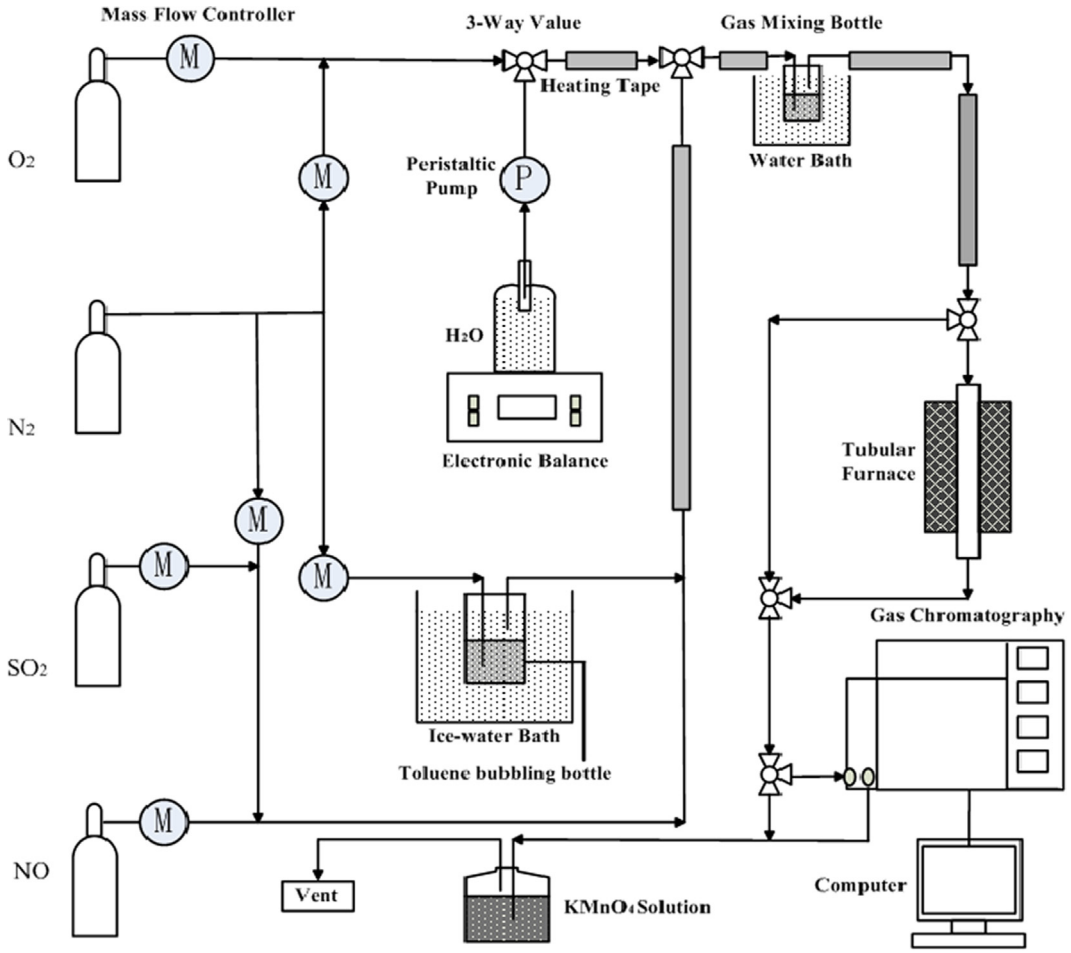

Fig. 1. Schematic diagram of the experimental setup.

MIRA3 LMU (China) instrument. The Brunauer-Emmett-Teller (BET) surface area, pore volume and average pore diameter of catalysts were obtained from N_2 adsorption isotherm using a Quadrasorb SI-3MP (USA). X-ray photoelectron spectroscopy (XPS, Thermo Fisher Scientific, USA) analyzed the chemical states of constituent elements on the sample surface. Temperature-Programmed Reduction of H_2 (H_2-TPR, AutoChem 2920 automated adsorption analyzer, China) was performed to monitor the redox properties of the metal oxide over samples. Oxygen temperature-programmed desorption (O_2-TPD) was conducted on chemisorption apparatus. More detailed characterization methods are provided in the Supporting Information.

2.3. Experimental setup and procedure

The performance of the prepared samples for elimination of toluene was evaluated on a vertical fixed bed tubular quartz reactor (6 mm inner diameter × 600 mm length) operating at continual flux at atmospheric pressure, and the schematic diagram of samples performing for toluene removal is shown in Fig. 1. The gas-phase toluene was produced from a bubbling bottle which was immersed in an ice-water bath. The reaction flue gas contained 500 ppm toluene, 6 vol% O_2 and pure N_2 as balance. The total volume of the feed flue gas was maintained at 200 mL/min for each test, and 0.50 g sample (40–60 mesh) was used, which resulted in a corresponding gas hourly space velocity (GHSV) of 15000 h^{-1}. The sample was placed in the middle of the reactor, with a thermocouple to monitor the reaction temperature of 150–300 °C. All of the tests were carried out three replicates to reproduce the results and reduce experimental error. The test was carried out under the condition of automatic programmed temperature, and the temperature remains unchanged for 3 h at the set temperature point. For instance, after the efficiency test of Mn_6Cu_5/AC treatment of toluene at 150 °C for 3 h, the temperature of the reaction bed was automatically raised to 180 °C at a heating rate of 5 °C/min, and the efficiency of 180 °C was obtained after treatment for 3 h. In addition, all of the reaction data was collected three times to reduce experimental error and all reported data was measured in a steady-state.

The toluene concentration of inlet and outlet were monitored by an on-line gas chromatograph (GC, GC-2014C, SHIMADZU) equipped with a flame ionization detector (FID) and a wax column (1 um, 0.32 mm Φ × 60 m). The efficiency of toluene removal was calculated based on the disappearance of toluene by means of the gas chromatography (GC). Prior to the formal test, a blank test was carried out to minimize the influence of the reactor and sample-itself. More details of the experiment procedures are provided in the Supporting Information.

The removal efficiency of toluene ($E_{toluene}$) was calculated as follows:

$$E_{toluene}(\%) = \frac{\Delta toluene}{toluene_{in}} = \frac{toluene_{in} - toluene_{out}}{toluene_{in}} \times 100\% \quad (1)$$

where $toluene_{in}$ = input concentration and $toluene_{out}$ = output concentration of toluene (ppm), according to the chromatograms.

2.4. In situ DRIFT investigation

The in situ diffuse reflectance FTIR spectra (DRIFT) of the prepared samples were collected in the range of 500–4000 cm^{-1} on a Thermo Fisher Nicolet iZ10 FTIR spectrometer equipped with a liquid N_2-cooled MCT detector. The pretreated sample was exposed to the corresponding

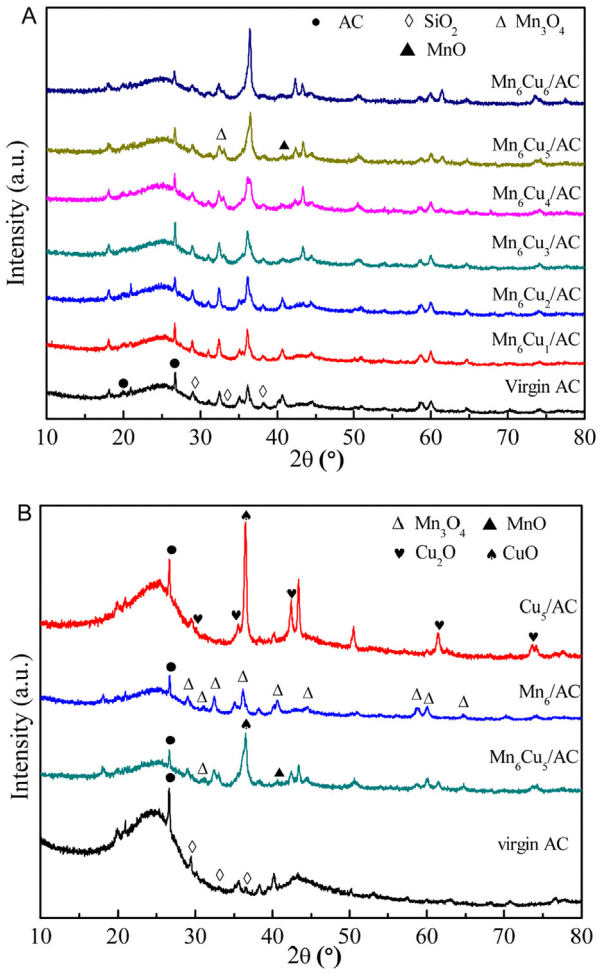

Fig. 2. XRD patterns of (A) Mn_6Cu_y/AC, (B) Cu_5/AC, Mn_6/AC and Mn_6Cu_5/AC.

gas atmosphere of toluene (500 ppm toluene + N_2) at 270 °C and toluene + O_2 (500 ppm toluene + 6% O_2 + N_2) at 270 °C, for 2 h to be measured, respectively. More detailed characterization methods are provided in the Supporting Information.

3. Results and discussion

3.1. Characterization of materials

3.1.1. Textural, structural and morphologic characterizations

The X-ray diffraction profiles of the virgin AC and Mn_xCu_y/AC are presented in Fig. 2A. With regards to virgin AC, a group of characteristic signals of carbon (2θ = 26.68° and 44.50°, PDF-ICDD 25-0248) and SiO_2 (2θ = 28.89°, 32.22° and 36.04°, PDF-ICDD 18-1170) were detected. And the intensity of the characteristic peaks were decreased as the concentration of Mn and Cu oxides over the AC, which may suggested the change of AC pristine structure on account of the interaction between Mn-Cu oxides and AC [40]. As shown in Fig. 2B, for Cu_5/AC, four peaks at 2θ = 36.38°, 42.46°, 61.46° and 73.62° (PDF-ICDD 65-3288) belonged to the main phase Cu_2O were detected, while the distinct reflection at 2θ = 36.58° could be ascribed to monoclinic CuO (PDF-ICDD 48–1548) [41]. This indicated Cu_2O and CuO coexisted over the sample. In the case of Mn_6/AC, the major diffraction peaks at 2θ = 29.12°, 31.14°, 32.54°, 36.20° and 44.46° were consistent with the characteristic peaks of Mn_3O_4 (PDF-ICDD 24-0734), and the diffraction peak at 2θ = 40.86° was attributed to MnO (PDF-ICDD 07-0230) [32]. Notably, the diffraction peaks of Mn_3O_4 in a series of Mn_6Cu_y/AC were significantly weaker than that in Mn_6/AC. This demonstrated the addition of CuO_x prevented manganese oxides from reaching a crystalline structure, which might be attributed to the interaction between copper and manganese oxides. The synergistic interaction has been reported by Cao to lead to the improvement of oxygen vacancies, and presumably the subsequent high catalytic activity [42]. Nevertheless, further increasing Cu content to y > 5 led to a slight increase in crystallinity, which demonstrates that an appropriate amount of the CuO_x may have a favorable dispersing effect on manganese species.

SEM micrographs of nine as-prepared samples are shown in Fig. 3. The image of Cu_5/AC clearly displayed that the surface particles had a shuttle shape, while randomly distributed spherical grains along with agglomerates were explicitly obtained over Mn_6/AC [43]. Moreover, the surface morphology of the samples gradually evolved from particles to strip through the intermediate state of the flat blocks from Fig. 3(d)–(i), which is believed to be resulting from the interaction between MnO_x and CuO_x caused by the increasing Cu content. This was in line with the XRD results. Particularly, a well dispersed cluster-like agglomerates composed of thin rods were formed on the surface of Mn_6Cu_5/AC, and the diameter was finer and the size distribution was more homogeneous than Mn_6Cu_6/AC. Furthermore, result of EDX (Fig. S1, see detailed in Supporting Information) illustrated MnO_x was easier to agglomeration than CuO_x. In addition, ICP-AES (Table S1) results demonstrated that the metals were successfully loaded on AC accompanied by a slightly loss.

3.1.2. BET

The overall microstructural characteristic of as-prepared samples, including specific surface area, total pore volume and average pore diameter, were characterized by BET. As shown in Table 1, all modified samples possessed larger specific surface area than virgin AC, moreover, that of the co-modification samples was higher than the sample separately loaded with manganese (224.41 m^2/g) or copper (221.87 m^2/g), which presumably illustrated that the synergistic effect between CuO_x and MnO_x are beneficial to the increase of BET surface area [44]. Nevertheless, the surface area was decreased with the content of loaded Cu increased except for Mn_6Cu_4/AC. According to Tao [45], the reduction may be associated with the aggregation of excess loaded metal oxides on the surface of samples, and became more pronounced as the load increase. Besides, the Mn-Cu modified AC possessed higher pore volume and smaller average pore diameter than virgin AC. It might be ascribed to some new pores were formed due to the removal of volatiles during the impregnation and calcination process as well as the disordered stacking of loaded active components [46]. Combined with SEM and BET, the structure of Mn_6Cu_5/AC could offer large surface areas, therefor more active surface areas, resulting in abundant defects and strong interactions. In addition, the pore size distribution curves (Fig. S2.) show that the prepared catalysts were mesoporous material with a pore size of 2–3 nm, then the effective adsorption channels for toluene can be provided [20].

3.1.3. XPS

XPS analysis was used to illuminate the chemical states as well as the composition of different species over the samples. XPS spectra of C 1s are plotted in Fig. 4(a). The asymmetric photoelectron peak can be deconvolution into four peaks belonging to graphitic carbon (284.66–284.71 eV), phenolic, alcoholic or etheric functional groups (285.52–285.77 eV), carbonyl or quinone functional groups (287.59–287.73 eV), carboxyl or ester functional groups (289.04–290.82 eV) [47], respectively. From the results of Table 2, after the loading of metal oxides, the ratio of COO increased by 3.61% compared with the virgin AC, which may be due to nitrate was used as a precursor for immersion, as reported in the literature [27]. However, the proportion of C—O— and C═O decreased by 4.03% and 1.64%, respectively. According to Huang [48], the decrease may be due to the reaction of AC with the precursors during the treatment process.

Three kinds of oxygen species were detected as shown in Fig. 4(b),

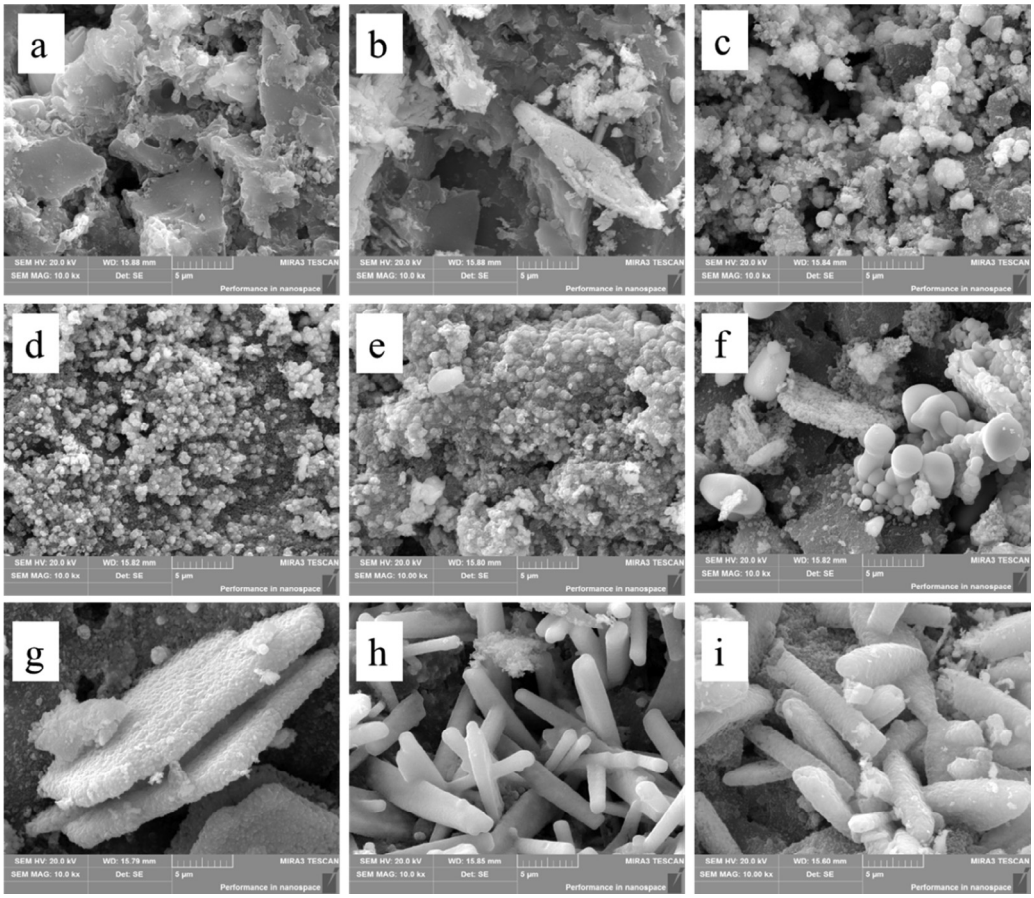

Fig. 3. SEM images (×10,000) of (a) virgin AC, (b) Cu_5/AC, (c) Mn_6/AC, (d) Mn_6Cu_1/AC, (e) Mn_6Cu_2/AC, (f) Mn_6Cu_3/AC, (g) Mn_6Cu_4/AC, (h) Mn_6Cu_5/AC, (i) Mn_6Cu_6/AC.

Table 1
BET surface and pore parameters of different samples.

Sample	BET surface area (m^2/g)	Total pore volume (cm^3/g)	Average diameter (nm)
AC	153.11	0.095	2.485
Cu_5/AC	221.87	0.126	2.269
Mn_6/AC	224.41	0.142	2.530
Mn_6Cu_1/AC	250.24	0.135	2.155
Mn_6Cu_2/AC	243.90	0.138	2.270
Mn_6Cu_3/AC	237.29	0.133	2.246
Mn_6Cu_4/AC	245.22	0.143	2.336
Mn_6Cu_5/AC	235.95	0.139	2.368
Mn_6Cu_6/AC	233.40	0.138	2.362

the O 1s signal with binding energy (BE) from 529.9 to 530.9 eV, 531.4–532.5 eV and 532.6–534.0 eV was characteristic of lattice oxygen (denoted as O_A), surface adsorbed oxygen and oxygen vacancies (denoted as O_B) and the oxygen species (denoted as O_C) were derived from hydroxyl species and adsorbed molecular water on the surface [49–52], respectively. In addition, the O_A, O_B and O_C ratio of the samples were calculated by O_A/O_T, O_B/O_T and O_C/O_T ($O_T = O_A + O_B + O_C$), and the relevant data is summarized in Table 2. As can be observed, the ratio of O_A and O_B over modified samples was increased compared with virgin AC. The amount of O_B on Mn_6Cu_5/AC (66.98%) was remarkably increased compared with Mn_6/AC (41.90%) and Cu_5/AC (48.25%), which indicated that the interaction between MnO_x and CuO_x was in favor of the generation of O_B. However, O_C was decreased in modified samples attributed to the volatilization of water over AC during the calcination process [39,53].

In the high-resolution of Cu 2p spectra (Fig. 4(c)), Cu $2p_{1/2}$ (953–957 eV), Cu $2p_{3/2}$ (933–937 eV) peaks species and satellite peaks (centered at 943–945 eV and 962–964 eV, respectively) were observed for fresh/used Mn_6Cu_5/AC and Cu_5/AC [34]. For Cu_5/AC, Cu 2p located at ca. 934.2 and 954.1 eV with an asymmetric character was Cu^+, whereas Cu^{2+} appeared at ca. 936.1 and 956.1 eV, accompanying with two shake-up satellites. While after doping of MnO_x, the interaction between CuO_x and MnO_x resulted in the B.E. of Mn_6Cu_5/AC was higher than Cu_5/AC; in addition, the ratio of Cu^+/Cu^{2+} increased from 0.95 to 1.22. As reported [53], Cu_2O had higher catalytic oxidation activity because it belonged to p-type semiconductor catalyst, capable of hole conduction and preferentially adsorbing O_2. Therefore, the existence of sufficient Cu^+ will be beneficial to the adsorption and activation of oxygen, thus improving the oxidation activity of the catalyst.

As seen from the Mn 2p core spectra in Fig. 4(d), the B.E. signals of Mn $2p_{3/2}$ around at 640.5–641.1 eV, 642.2–642.4 eV and 644.9–645.1 eV correspond to the surface Mn^{2+}, Mn^{3+} and Mn^{4+} species, respectively [54]. All the peaks of Mn_6Cu_5/AC turned to lower B.E. compared with Mn_6/AC and it was worth noting that the proportion of Mn^{4+} was increased to 28.19% after the doping of CuO_x. The ratios ranking of $Mn^{4+}/(Mn^{2+} + Mn^{3+} + Mn^{4+})$ was as follows: Mn_6/AC (0.29) < used Mn_6Cu_5/AC (0.39) < Mn_6Cu_5/AC (0.44), and it could be speculated that the incorporation of CuO_x could be in favor of the generation of high valance Mn atoms [55], the Mn^{4+} was the main active ion and played an important role in the catalytic reaction.

3.1.4. H_2-TPR

The reducibility of samples can be well characterized by H_2-TPR and the results are illustrated in Fig. 5. It was observed that virgin AC exhibited two overlapping peaks at 511 and 665 °C, ascribed to the reduction of surface adsorbed oxygen species and the gasification of the

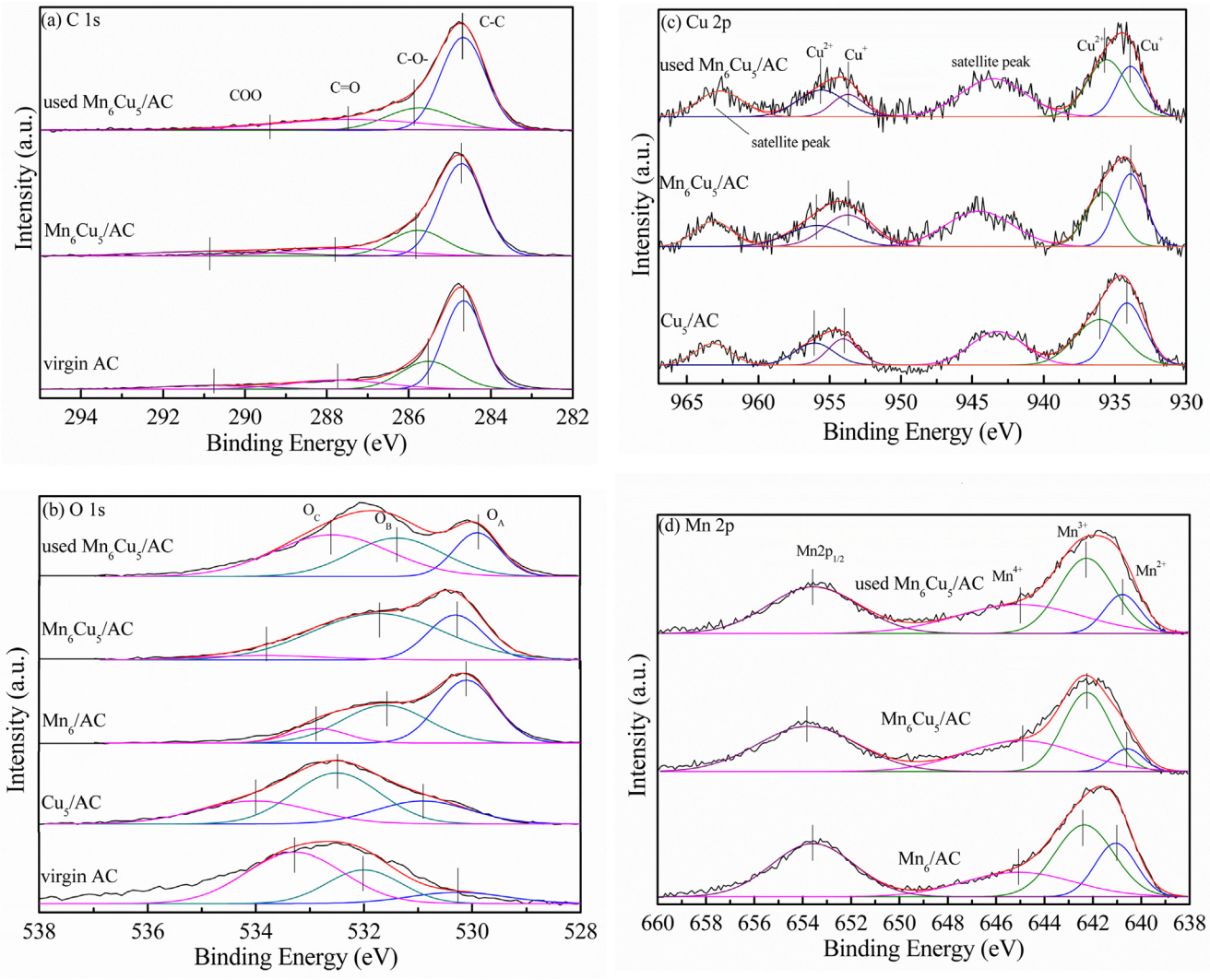

Fig. 4. XPS profiles corresponding to the samples before and after the reaction for (a) C 1s, (b) O 1s, (c) Cu 2p and (d) Mn 2p. (Reaction condition: 500 ppm toluene, 6% O_2, total flow rate 200 mL/min, reaction temperature 270 °C).

carbon support [56], respectively. Thus, all the peaks displayed at approximately 670 °C could be ascribed to AC support gasification. For Cu_5/AC, the peak at 399 °C was ascribed to the reduction of Cu^{2+} to Cu^{+}, and the another peak was attributed to the transformation of Cu^{+} to Cu^{0}, as well as the reduction of surface oxygen species [11,42]. The TPR profile of Mn_6/AC showed peaks at about 451 and 539 °C, these peaks probably correspond to the reduction of MnO_2 to MnO via an intermediate state of Mn_3O_4 as well as the reduction of surface oxygen species [27,57]. Obviously, the reduction peaks shifted towards lower temperature after loading of CuO_x or MnO_x compared with virgin AC,

Table 2
The relative XPS intensity of as-prepared samples.

Compositions (%)	AC	Cu_5/AC	Mn_6/AC	Mn_6Cu_5/AC	Used Mn_6Cu_5/AC
C—C	56.00	–	–	58.05	55.08
C—O—	24.51	–	–	20.48	19.85
C═O	13.81	–	–	12.17	21.85
COO	5.68	–	–	9.29	3.21
O_A	12.76	23.55	47.25	27.24	19.59
O_B	29.13	48.25	41.90	66.98	34.03
O_C	58.11	28.20	10.85	5.78	46.38
[a]Cu^{+}	–	34.17	–	36.63	23.39
[a]Cu^{2+}	–	36.11	–	30.13	37.49
Cu^{+}/Cu^{2+}	–	0.95	–	1.22	0.62
[b]Mn^{2+}	–	–	16.28	5.82	10.50
[b]Mn^{3+}	–	–	31.36	29.97	30.92
[b]Mn^{4+}	–	–	19.91	28.19	27.03
$Mn^{4+}/(Mn^{2+}+Mn^{3+}+Mn^{4+})$	–	–	0.29	0.44	0.39

[a] The percent of different valence of Cu in Cu $2p_{1/2}$ and Cu $2p_{3/2}$.
[b] The percent of different valence of Mn in Mn $2p_{3/2}$.

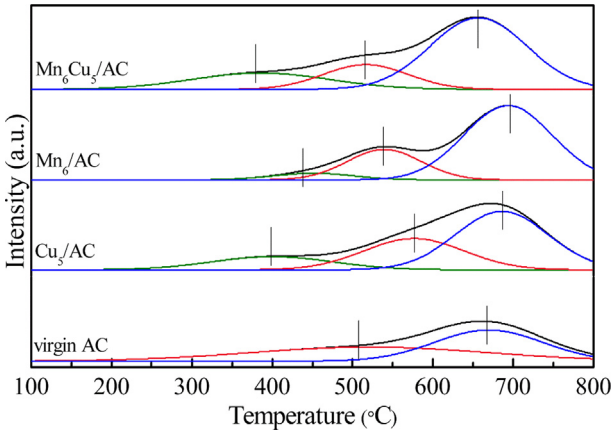

Fig. 5. H_2-TPR profiles of virgin AC, Cu_5/AC, Mn_6/AC and Mn_6Cu_5/AC.

manifesting the strong interaction between the loading composition and the support. The reduction of CuO_x and MnO_x in Mn_6Cu_5/AC took place at the lowest temperature, and the peak at 385 °C can be attributed to the CuO_x to Cu^0 which own the lower free energy, the peak at 516 °C can be ascribed to the reduction processes of $Mn^{4+} \rightarrow Mn^{3+} \rightarrow Mn^{2+}$ and surface oxygen species [58]. The lower reduction temperatures further attested the existence of strong synergistic interaction between MnO_x and CuO_x, and in good agreement with Morales's report that Cu may catalyze the reduction of manganese oxides in a Mn-Cu mixed oxide sample, which was conducive for the destruction of toluene [58]. As is known, a lower reduction temperature is accompanied by a higher catalytic activity [59]. Therefore, it can be speculated that Mn_6Cu_5/AC may showed the best activity for toluene oxidation. In addition, the inset image of in Fig. S3 shows the desorption peaks of O_2-TPD, in which a greater peak area and a lower desorption temperature was founded over Mn_6Cu_5/AC, it may lead to enhanced catalytic ability due to the more abundant and better mobility of active oxygen species.

3.2. Removal performance test of toluene

3.2.1. Effect of Mn loading

The toluene removal performance of the supported manganese oxide samples was evaluated at 150–330 °C to determine the optimum load of manganese oxide. The result of the blank test of toluene removal without catalyst shows that there was almost no difference in the inlet and outlet toluene concentration at 150–330 °C. Fig. 6 shows the

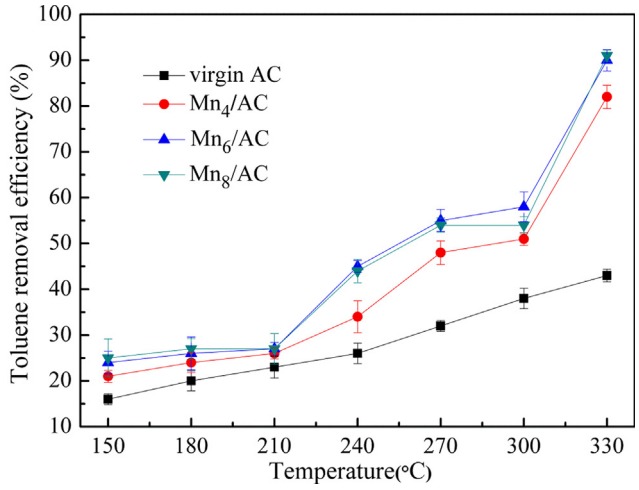

Fig. 6. Toluene conversion over different Mn loading on AC samples in flue gas. (Reaction condition: 500 ppm toluene, 6% O_2, 0.5 g sample, total flow rate 200 mL/min).

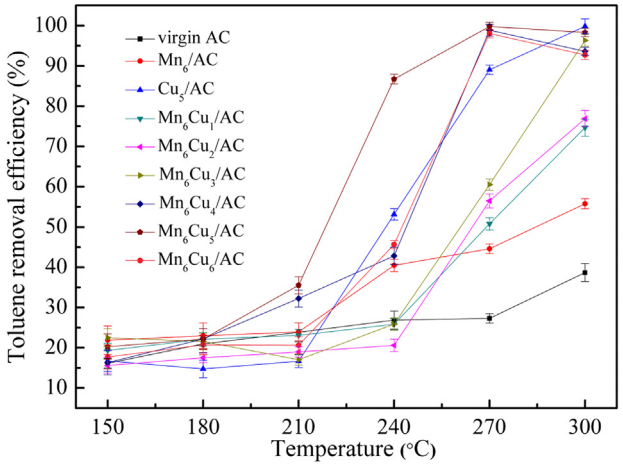

Fig. 7. Removal of toluene on Mn_6Cu_y/AC samples in flue gas. (Reaction condition: 500 ppm toluene, 6% O_2, 0.5 g sample, total flow rate 200 mL/min).

toluene removal efficiency for virgin AC, Mn_4/AC, Mn_6/AC and Mn_8/AC were obviously improved with rising reaction temperature. This was consistent with Liu's work [38] that the more reaction activation energy of reactants provided by higher temperature would assist for the elimination of toluene. Additionally, the phenomenon that the toluene removal efficiency improved by the increase of reaction temperature also indicated that the mechanism of toluene removal on AC, Mn_4/AC, Mn_6/AC and Mn_8/AC were not only adsorption, but also catalytic oxidation [35]. Obviously, Mn_x/AC showed the enhanced toluene removal efficiency than virgin AC (15–45%). In particular, the activity keep rising when the load of manganese was not more than 6 wt%, and then maintains relatively constant despite further increase Mn loading to 8 wt%. It might be due to the growth of crystalline size and surface blocking resulted from excessive Mn loading [60]. Therefore, the Mn_6/AC can be considered as the optimal Mn loading sample for consideration of operation cost and toluene removal efficiency.

3.2.2. Catalytic performance of Mn_xCu_y/AC samples

According to Section 3.2.1, a 6 wt% Mn loading was selected to determine the optimal Cu loading and the further factors affecting the activity of supported bimetal oxide sample. Fig. 7 shows the toluene catalytic efficiency of Mn_6Cu_y/AC initially increased with the increasing temperature, in particular, a significantly increased during 210–270 °C. Moreover, it was also noticed that CuO_x can synergize with MnO_x to improve the removal efficiency of toluene [61]. Thereinto, Mn_6Cu_5/AC showed the superior activity at low temperatures, further reached the maximum efficiency of 99.81% at 270 °C. It was further found that the toluene removal efficiency of Mn_6Cu_4/AC, Mn_6Cu_5/AC, Mn_6Cu_6/AC decreased at 300 °C and the slight sintering of catalyst should be responsible for the decrease. It is known that the catalytic oxidation of toluene is a strongly exothermic reaction, and the accumulation heat released during the catalytic oxidation of toluene will be superimposed with the temperature of the catalytic bed to form an excessively high temperature, which leads to the sintering of the catalyst [62]. For achieving the most excellent removal efficiency, 270 °C was selected as default operational condition in the following tests.

Generally, it is considered that there are several main factors determining the removal activity of sample such as morphologies, redox properties and oxygen mobility, derived from the nature of metals as well as improved by the optimized collaborative load. BET surface area (Table 1) played an important but not decisive role in the removal activity of samples based on the previous researches [42]. Although the reduced specific surface area was not conducive to the adsorption of toluene, the increased pore size is believed to be beneficial to reduce transfer resistance and improve further oxidized decomposed of

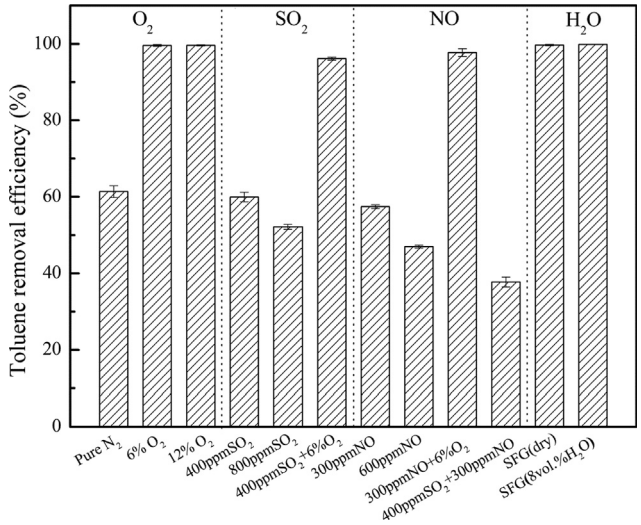

Fig. 8. Effect of flue gas components on toluene removal over Mn_6Cu_5/AC. (Reaction condition: 500 ppm toluene, 0–12% O_2, 0–800 ppm SO_2, 0–600 ppm NO, 0-8 vol% H_2O, 0.5 g sample, total flow rate 200 mL/min, reaction temperature 270 °C, and SFG = 500 ppm toluene + 300 ppm NO + 400 ppm SO_2 + 6% O_2 + balance N_2).

toluene. For example, Mn_6/AC with lower BET surface area, but with larger pore volume and pore diameter, had higher toluene removal efficiency than Mn_6Cu_1/AC, Mn_6Cu_2/AC and Mn_6Cu_3/AC when the temperature was below 210 °C. Besides, from the characterization result of H_2-TPR and O_2-TPD, the activity of sample was closely related to the reducibility and oxygen activation. Combination this with XPS characterization (Fig. 4), the higher efficiency of Mn_6Cu_5/AC can be derive from the improvement in the mobility as well as the amount of surface active oxygen and the increase of the amount of Cu^+ and Mn^{4+}. According to the aforementioned characterizations results, Mn_6Cu_5/AC sample possessed the unique microstructure, larger BET, more active sites, preferable low-temperature reducibility and good oxygen mobility ability, which were beneficial for toluene oxidation.

3.3. Effect of flue gas components

Effects of the flue gas components (O_2, SO_2, NO and H_2O) on toluene removal over Mn_6Cu_5/AC sample at 270 °C were demonstrated in Fig. 8.

3.3.1. Effect of O_2

The effect of different O_2 concentrations (0%, 6% and 12%) on $E_{toluene}$ were investigated, the results are shown in Fig. 8. It could be clearly seen that Mn_6Cu_5/AC still revealed a relatively high activity of 61.84% despite the absence of O_2 at 270 °C, which mainly attributed to the consumption of abundant O_A and O_B. However, a significant increase of $E_{toluene}$ was observed after the introduced of 6% O_2, which could be attributed to the O_A and O_B consumed during the removal process were regenerated and supplemented by gas-phase oxygen [28]. Furthermore, there was a negligible change in the removal efficiency of toluene when further increase the concentration of oxygen to 12%, because 6% O_2 was sufficient for the oxidation of toluene.

3.3.2. Effect of SO_2

In Fig. 8, three reaction conditions were carried out to examine the effect of SO_2 impurity on catalytic activity of Mn_6Cu_5/AC. It can be observed that Mn_6Cu_5/AC revealed a deteriorated catalytic performance compared with that of pure N_2 when SO_2 was introduced, and the negative effect increased with the enhancement of SO_2 concentration. For instance, Mn_6Cu_5/AC only revealed a performance of 59.93% and 52.16% with the introduction of 400 and 800 ppm SO_2 at the absence of O_2, respectively. The suppression of SO_2 might be ascribed into the competition with toluene for active sites. SO_2 (diameter = 0.41 nm) could be adsorbed on the surface of Mn_6Cu_5/AC and further generate a large number of sulfites and sulfates, which not only consumed the active sites but also caused the blockage of pores for toluene removal [34]. However, with the addition of 6% O_2 into the feed, the inhibition effect was weakened as a result of the replenishment of the O_A and O_B consumed by SO_2, which revealed a relatively sulfur-resistance of the Mn_6Cu_5/AC sample.

3.3.3. Effect of NO

As shown in Fig. 8, toluene removal efficiencies were 57.41% and 46.98% in the presence of 300 and 600 ppm NO balanced in N_2, respectively, which was declined compared with that of pure N_2. Similar to SO_2, NO molecules could occupy active sites and react with labile surface oxygen to facilitate the formation of NO_2, even NO_2^- and NO_3^- [27,40]. Although the generated NO_2 could be used for the subsequently toluene activation, the inhibitory was still evident because of the occupation of active sites and the consumption of active oxygen species [63]. However, after adding 6% O_2 to the feed gas containing 300 ppm NO, the removal efficiency of toluene was enhanced to 97.75%, which was not only attributed to the timely replenished of active oxygen species but also the more produced NO_2 as a more powerful oxidant [34,64]. In addition, the toluene removal efficiency was 37.73% when SO_2 and NO coexisted in the feed gas without O_2, which was caused by the strengthened competition between NO, SO_2 and toluene. With the introduction of 6% O_2, a high toluene removal efficiency, almost as efficient as in N_2 + O_2 + toluene atmosphere, was obtained over Mn_6Cu_5/AC, which demonstrating that Mn_6Cu_5/AC has great potential in practical application.

3.3.4. Effect of H_2O

In order to further examine the possible application of catalyst in real exhaust condition, the influence of the presence of 8 vol% H_2O in the simulated flue gas (SFG) was evaluated. Generally speaking, there will be a negative effect on the catalytic activity due to the competition for active sites between water molecules and toluene molecules [52]. However, as shown in Fig. 8, water vapor had no obvious inhibition for the toluene removal because the efficiency remained almost constant. On the one hand, the hydrophobicity of activated coke carrier will reduce the competition of active sites between water and toluene; on the other hand, Li et al. also found that water could act as a hydrolysis agent and hydrogen-supplying agent to facilitate the conversion of toluene [64]. Therefore, it can be speculated that the addition of water may have an effect on the intermediate products to a certain extent instead of the final efficiency. It also suggested Mn_6Cu_5/AC possesses excellent H_2O resistance, which is competitive in practical application on catalytic removal of toluene.

3.4. The reusability and durability of Mn_6Cu_5/AC sample

Three consecutive catalytic runs and long-term catalytic performance of toluene eliminate were evaluated of the best-performing Mn_6Cu_5/AC catalyst. In Fig. 9(a), there was a slight decrease in activity of Mn_6Cu_5/AC over three times cycles, and the efficiency of the second cycle was basically consistent with that of the third cycle, which manifested that Mn_6Cu_5/AC exhibited good catalytic reusability. Same as the analysis in Section 3.2.2, the sintering at high temperature of Mn_6Cu_5/AC should be responsible for the decrease of toluene removal efficiency during the second and third cycle. As shown in Fig. 9(b), the toluene removal efficiency still remained above 81% with the reaction time extended to 30 h, which showed that the catalyst had a long lifetime and excellent performance. All the results suggested that Mn_6Cu_5/AC was catalytically reusable and durable for toluene oxidation and the reusability and long-term good stability provided the possibility for the practical elimination of VOCs.

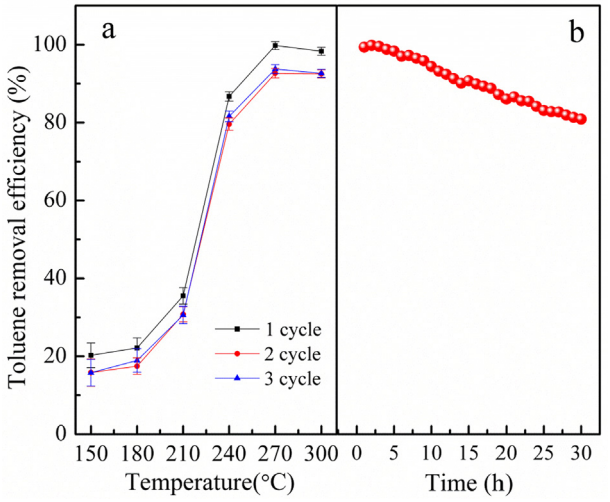

Fig. 9. The reusability and durability of Mn_6Cu_5/AC sample: (a) toluene removal efficiency curves for three consecutive cycles from 150 to 300 °C; (b) durability test of toluene removal at 270 °C. (Reaction condition: (a) 500 ppm toluene, 6% O_2, and balance N_2, 0.5 g sample, total flow rate 200 mL/min; (b) 500 ppm toluene, 300 ppm NO, 400 ppm SO_2, 6% O_2, 8 vol% H_2O and balance N_2, 0.5 g sample, total flow rate 200 mL/min).

3.5. The mechanism for catalytic oxidation of toluene over Mn_6Cu_5/AC

The chemical states of fresh and used Mn_6Cu_5/AC were investigated by XPS. After treated with toluene, C—O— and COO showed a decrease compared with the fresh sample, which implied the participated in the toluene removal process. And the increase in C═O may be due to the formation of the intermediates containing C═O in toluene oxidation. For O 1s, a significant decrease of O_A (7.65%) and O_B (32.95%) was accompanied by the use of Mn_6Cu_5/AC, manifesting that both O_A and O_B participated in toluene removal as active oxygen species. And according to the previous report [28], O_B was well connected with the toluene removal efficiency. This strongly suggests that surface adsorbed oxygen and oxygen vacancies, which were considered to be the most active oxygen species because of their high mobility [50,51]. Besides, an increase of 40.60% for O_C might reveal an amount of H_2O was generated during toluene decomposition and oxidation. In addition, the ratio of Cu^+/Cu^{2+} over Mn_6Cu_5/AC decreased from 1.22 to 0.62 after participated in toluene removal reaction, which could deduce that the oxidation of Cu^+ was occurred during the reaction process. Besides, the ratio of Mn^{4+} decreased by 1.16%, while more Mn^{2+} and Mn^{3+} were generated after treated with toluene, suggesting a redox reaction took place in the toluene oxidation process, which also indicated that Mn^{4+} participated in the reaction.

In order to elucidate the precise reaction mechanism of toluene over Mn_6Cu_5/AC, in situ DRIFT spectra, which could dynamically monitor the reaction intermediates and products in time sequence, was subsequently carried out (Fig. 10).

In situ DRIFTS spectra for Mn_6Cu_5/AC were firstly recorded in 500 ppm toluene/N_2 flow at 270 °C to explore the catalytic behavior of O_A and O_B in toluene oxidation. The DRIFTS spectra of surface species over Mn_6Cu_5/AC are demonstrated in Fig. 10(a). The typical in-plane skeletal vibrations of the aromatic ring at 1496 and 1611 cm^{-1} were immediately observed over Mn_6Cu_5/AC once in contact with toluene, where in-plane toluene C—H bending were also observed at 724, 1029 and 1075 cm^{-1} [10]. In the C—H stretching region (3100–2850 cm^{-1}), the bands at 3072, 3036, 2932, 2887 cm^{-1} were detected. Thereinto, the bands at 3072 and 3036 cm^{-1} could be assigned to the $\nu_{C\text{-}H}$ of aromatic ring, the bands at 2932 and 2887 cm^{-1} could be ascribed to the symmetric or asymmetric $\nu_{C\text{-}H}$ of methyl group for toluene [18,65]. The intensity of these peaks monotonically increased with time, which

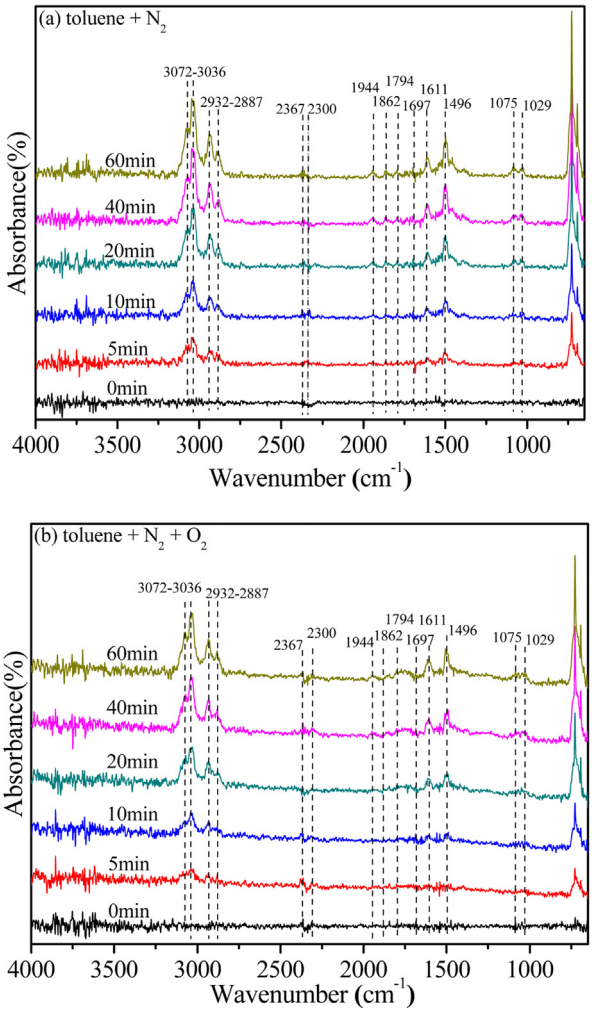

Fig. 10. In situ DRIFTS analysis on Mn_6Cu_5/AC catalyst under different conditions: (a) 500 ppm toluene + N_2 as balance at 270 °C; (b) 500 ppm toluene + 6% O_2 + N_2 as balance at 270 °C.

implies that toluene continuous to adsorb over sample surface at a rate greater than that of oxidation. In addition, a new characteristic IR band corresponding to C═O stretching vibration of benzaldehyde appearance at 1697 cm^{-1} [66], possibly indicating that toluene was partially oxidation by the active oxygen species originating from Mn_6Cu_5/AC [66]. Furthermore, the peaks of 1794, 1862, 1944 cm^{-1} were considered as the symmetric stretching vibration of maleic anhydride [65], which most probably indicated that benzene ring was opened and transformed into maleic anhydride. Also, the antisymmetric stretching vibration bands of CO_2 at 2300 and 2367 cm^{-1} were identified, which was the final oxidation state of toluene. It indicated that the Mn_6Cu_5/AC could act as an efficient catalyst with sufficient active oxygen species for toluene oxidation even in the absence of O_2. Upon the introduction of O_2, similar bands were observed in Fig. 10(b). As shown, the relative intensity of bands at 3100–2850 cm^{-1}, 1075 and 1029 cm^{-1} attributed to toluene become weaker, and the bands at 1697 cm^{-1} and 2300, 2367 cm^{-1} assigned to C═O stretching vibration of benzaldehyde and antisymmetric stretching vibration bands of CO_2 were strengthened, respectively. In general, the amount of the intermediates on the catalyst surface depends on both the formation rate of adsorbed toluene and its deep oxidation rate. Therefore, the results indicated that the introduction of gas-phase O_2 could significantly accelerate the transformation of adsorbed toluene to intermediate species, even CO_2, by supplementing the surface active oxygen, which was consistent with the experimental results of the effect of O_2 in Section

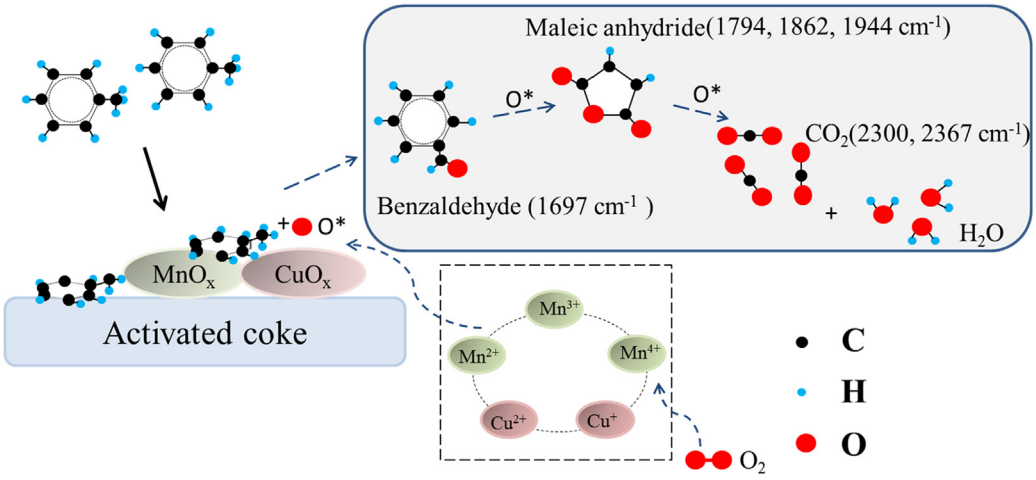

Fig. 11. The proposed mechanism of toluene removal process over Mn_6Cu_5/AC.

3.3.1.

On the basis of the characterizations and obtained results in this work, a possible reaction mechanism for toluene remove over Mn_6Cu_5/AC was proposed, as shown in Fig. 11. During the oxidation process, toluene was firstly adsorbed on the catalyst surface, and then reacted with active oxygen species on Mn_6Cu_5/AC surface, sequentially resulting in the formation of benzaldehyde species. Then, accompanying with the cleavage of aromatic ring, the oxidation products were further oxidized to maleic anhydrides by active oxygen species. Finally, the maleic anhydrides were oxidized into CO_2. It should be mentioned that oxygen vacancies play a vital role in the whole process, because oxygen vacancies can be formed and then be filled by the decomposition of gas-phase O_2 rapidly, accelerating the bond cleavage of reactants via the lower oxygen migration activation energy [67].

4. Conclusion

The catalytic activities of toluene over the supported different wt% manganese oxide samples were in the order of Mn_6/AC ≥ Mn_8/AC > Mn_4/AC. Mn_6/AC was chosen as the basis to determine the optimum copper contents to be added on. It was confirmed that Mn_6Cu_5/AC had outstanding performances with 99.38% toluene removal efficiency at 270 °C and presented satisfactory reusability and durability under simulated flue gas. SO_2 and NO played a hindering role in the removal of toluene in the absence of O_2 due to the competitive adsorption of active sites, whereas the negative effect would be reduced due to the introduction of O_2. It was concluded that gas-phase O_2 could replenish the consumed surface active oxygen, which played a crucial role in the oxidation of toluene. Besides, the introduction of H_2O in the feed had no significant influence on toluene removal. According to the various characterization results, the performance enhancement of Mn_6Cu_5/AC was probably ascribed to the synergistic interaction between manganese oxide and copper oxide, which lead to the homogeneous distribution and morphology (XRD and SEM), the large specific surface area (BET), the strong reducibility (H_2-TPR) and the good oxygen mobility ability (O_2-TPD). Moreover, the XPS results indicated that due to the synergistic effect between MnO_x and CuO_x, more active oxygen species was formed, as well as the greater quantities of monovalent copper ions and tetravalent manganese ions, which were favorable to the removal of toluene. Furthermore, the possible reaction process of toluene oxidation on Mn_6Cu_5/AC was also investigated by DRIFTS. The reaction process indicated that toluene could be rapidly adsorbed and activated to form the benzaldehyde and maleic anhydride species on the surfaces of Mn_6Cu_5/AC, and finally further oxidized into CO_2. Further studies to investigate the mechanism how NO, SO_2 and H_2O affect toluene removal are warranted.

CRediT authorship contribution statement

Yindi Zhang: Methodology, Formal analysis, Investigation, Writing - original draft, Data curation. **Caiting Li:** Supervision, Writing - review & editing. **Youcai Zhu:** Writing - review & editing. **Xueyu Du:** Writing - review & editing. **Yue Lyu:** Writing - review & editing. **Shanhong Li:** Supervision. **Yunbo Zhai:** Supervision.

Declaration of Competing Interest

The authors declare that they have no known competing financial interests or personal relationships that could have appeared to influence the work reported in this paper.

Acknowledgements

This work was supported by the National Key Research and Development Program of China (2016YFC0204100) and the Key Research and Development Program of Hunan Province in China (2018SK2032).

Appendix A. Supplementary data

Supplementary data to this article can be found online at https://doi.org/10.1016/j.fuel.2020.118099.

References

[1] Garcia JP, Beyne-Masclet S, Mouvier G. Emissions of volatile organic compounds by coal-fired power stations. Atmos Environ 1992;26:1589–97.
[2] Suárez-Vázquez SI, Gil S, García-Vargas JM, Cruz-López A, Giroir-Fendler A. Catalytic oxidation of toluene by $SrTi_{1-x}B_xO_3$ (B = Cu and Mn) with dendritic morphology synthesized by one pot hydrothermal route. Appl Catal B: Environ 2018;223:201–8.
[3] Amann M, Lutz M. The revision of the air quality legislation in the European union related to ground-level ozone. J Hazard Mater 2000;78:41–62.
[4] Du J, Qu Z, Dong C, Song L, Qin Y, Huang N. Low-temperature abatement of toluene over Mn-Ce oxides catalysts synthesized by a modified hydrothermal approach. Appl Surf Sci 2018;433:1025–35.
[5] Zhang J, Rao C, Peng H, Peng C, Zhang L, Xu X, et al. Enhanced toluene combustion performance over Pt loaded hierarchical porous MOR zeolite. Chem Eng J 2018;334:10–8.
[6] Zhao S, Hu F, Li J. Hierarchical core-shell Al_2O_3@Pd-CoAlO microspheres for low-temperature toluene combustion. ACS Catal 2016;6:3433–41.
[7] Chen C, Zhu J, Chen F, Meng X, Zheng X, Gao X, et al. Enhanced performance in catalytic combustion of toluene over mesoporous Beta zeolite-supported platinum catalyst. Appl Catal B: Environ 2013;140–141:199–205.
[8] Zhao L, Zhang Z, Li Y, Leng X, Zhang T, Yuan F, et al. Synthesis of Ce_aMnO_x hollow microsphere with hierarchical structure and its excellent catalytic performance for toluene combustion. Appl Catal B: Environ 2019;245:502–12.
[9] Chen X, Chen X, Yu E, Cai S, Jia H, Chen J, et al. In situ pyrolysis of Ce-MOF to

prepare CeO_2 catalyst with obviously improved catalytic performance for toluene combustion. Chem Eng J 2018;344:469–79.
[10] Zhao C, Hao Q, Zhang Q, Yan N, Liu J, Dou B, et al. Catalytic self-sustained combustion of toluene and reaction pathway over $Cu_xMn_{1-x}Ce_{0.75}Zr_{0.25}/TiO_2$ catalysts. Appl Catal A 2019;569:66–74.
[11] Luo Y, Zheng Y, Zuo J, Feng X, Wang X, Zhang T, et al. Insights into the high performance of Mn-Co oxides derived from metal-organic frameworks for total toluene oxidation. J Hazard Mater 2018;349:119–27.
[12] The clean air act amendments 1990. A Guide for small businesses, US, EPA, September 1992.
[13] Gupta VK, Verma N. Removal of volatile organic compounds by cryogenic condensation followed by adsorption. Chem Eng Sci 2002;57:2679–96.
[14] Gil RR, Ruiz B, Lozano MS, Martín MJ, Fuente E. VOCs removal by adsorption onto activated carbons from biocollagenic wastes of vegetable tanning. Chem Eng J 2014;245:80–8.
[15] Guo YF, Dai-Qi YE, Chen KF. Catalysis-assisted non-thermal plasma technology for decomposition of volatile organic compounds(VOCs). Ind Catal 2005;13:1–5.
[16] Everaert K, Baeyens J. Catalytic combustion of volatile organic compounds. J Hazard Mater 2004;109:113–39.
[17] Chen X, Chen X, Cai S, Chen J, Xu W, Jia H, et al. Catalytic combustion of toluene over mesoporous Cr2O3-supported platinum catalysts prepared by in situ pyrolysis of MOFs. Chem Eng J 2018;334:768–79.
[18] Rui Z, Tang M, Ji W, Ding J, Ji H. Insight into the enhanced performance of TiO_2 nanotube supported Pt catalyst for toluene oxidation. Catal Today 2017;297:159–66.
[19] Bai B, Qiao Q, Li J, Hao J. Progress in research on catalysts for catalytic oxidation of formaldehyde. Chin J Catal 2016;37:102–22.
[20] Yang X, Yu X, Lin M, Ma X, Ge M. Enhancement effect of acid treatment on Mn_2O_3 catalyst for toluene oxidation. Catal Today 2019;327:254–61.
[21] Liu Y, Dai H, Deng J, Du Y, Li X, Zhao Z, et al. In situ poly (methyl methacrylate) templating generation and excellent catalytic performance of MnO_x/3DOM $LaMnO_3$ for the combustion of toluene and methanol. Appl Catal B: Environ 2013;140–141:493–505.
[22] Saqer SM, Kondarides DI, Verykios XE. Catalytic oxidation of toluene over binary mixtures of copper, manganese and cerium oxides supported on γ-Al_2O_3. Appl Catal B: Environ 2011;103:275–86.
[23] Zhou G, He X, Liu S, Xie H, Fu M. Phenyl VOCs catalytic combustion on supported CoMn/AC oxide catalyst. J Ind Eng Chem 2015;21:932–41.
[24] Chen J, Chen X, Xu W, Xu Z, Chen J, Jia H, et al. Hydrolysis driving redox reaction to synthesize Mn-Fe binary oxides as highly active catalysts for the removal of toluene. Chem Eng J 2017;330:281–93.
[25] Delimaris D, Ioannides T. VOC oxidation over CuO–CeO_2 catalysts prepared by a combustion method. Appl Catal B: Environ 2009;89:295–302.
[26] Sihaib Z, Puleo F, Garcia-Vargas JM, Retailleau L, Descorme C, Liotta LF, et al. Manganese oxide-based catalysts for toluene oxidation. Appl Catal B: Environ 2017;209:689–700.
[27] Du X, Li C, Zhao L, Zhang J, Gao L, Sheng J, et al. Promotional removal of HCHO from simulated flue gas over Mn-Fe oxides modified activated coke. Appl Catal B: Environ 2018;232:37–48.
[28] Chen J, Li C, Li S, Lu P, Gao L, Du X, et al. Simultaneous removal of HCHO and elemental mercury from flue gas over Co-Ce oxides supported on activated coke impregnated by sulfuric acid. Chem Eng J 2018;338:358–68.
[29] Liu Z, Li W. Catalytic activity and deactivation of toluene combustion on rod-like copper-manganese mixed oxides. Acta Phys.- Chim. Sin 2016;32:1795–800.
[30] Ahn C-W, You Y-W, Heo I, Hong JS, Jeon J-K, Ko Y-D, et al. Catalytic combustion of volatile organic compound over spherical-shaped copper–manganese oxide. J Ind Eng Chem 2017;47:439–45.
[31] Dey S, Dhal GC, Mohan D, Prasad R, Gupta RN. Cobalt doped $CuMnO_x$ catalysts for the preferential oxidation of carbon monoxide. Appl Surf Sci 2018;441:303–16.
[32] Liu P, Wei G, Liang X, Chen D, He H, Chen T, et al. Synergetic effect of Cu and Mn oxides supported on palygorskite for the catalytic oxidation of formaldehyde: Dispersion, microstructure, and catalytic performance. Appl Clay Sci 2018;161:265–73.
[33] Solsona B, Garcia T, Agouram S, Hutchings GJ, Taylor SH. The effect of gold addition on the catalytic performance of copper manganese oxide catalysts for the total oxidation of propane. Appl Catal B: Environ 2011;101:388–96.
[34] Wang Y, Yang D, Li S, Zhang L, Zheng G, Guo L. Layered copper manganese oxide for the efficient catalytic CO and VOCs oxidation. Chem Eng J 2019;357:258–68.
[35] Varez-merino MAAL, Ribeiro MF, Silva JM, Carrasco-marian F, Maldonado-hoadar FJ. Activated carbon and tungsten oxide supported on activated carbon catalysts for toluene catalytic combustion. Environ Sci Technol 2004;38:4664–70.
[36] Wu H, Li C, Zhao L, Zhang J, Zeng G, Xie YE, Zhang X, Wang Y. Removal of gaseous elemental mercury by cylindrical activated coke loaded with CoO_x-CeO_2 from simulated coal combustion flue gas. Energy Fuels 2015;29:6747–57.
[37] Du J, Yuan Y. Synthetic courses and influence factors in the synthesis of mesoporous materials with surfactant template method. J Yanbei Normal Univ 2004;20:46–8.
[38] Liu M, Li C, Zeng Q, Du X, Gao L, Li S, et al. Study on removal of elemental mercury over MoO_3-CeO_2/cylindrical activated coke in the presence of SO_2 by Hg-temperature-programmed desorption. Chem Eng J 2019;371:666–78.
[39] Sheng J, Li C, Zhao L, Du X, Gao L, Zeng G. Efficient removal of HCHO from simulated coal combustion flue gas using CuO-CeO_2 supported on cylindrical activated coke. Fuel 2017;197:397–406.
[40] Gao L, Li C, Lu P, Zhang J, Du X, Li S, et al. Simultaneous removal of Hg^0 and NO from simulated flue gas over columnar activated coke granules loaded with La_2O_3-CeO_2 at low temperature. Fuel 2018;215:30–9.
[41] Hosseini SA, Niaei A, Salari D, Alvarez-Galvan MC, Fierro JLG. Study of correlation between activity and structural properties of Cu-(Cr, Mn and Co)$_2$ nano mixed oxides in VOC combustion. Ceram Int 2014;40:6157–63.
[42] Cao H, Li X, Chen Y, Gong M, Wang J. Effect of loading content of copper oxides on performance of Mn-Cu mixed oxide catalysts for catalytic combustion of benzene. J Rare Earths 2012;30:871–7.
[43] Ye Z, Giraudon JM, Nuns N, Simon P, De Geyter N, Morent R, et al. Influence of the preparation method on the activity of copper-manganese oxides for toluene total oxidation. Appl Catal B: Environ 2018;223:154–66.
[44] Yi H, Yang X, Tang X, Zhao S, Wang J, Cui X, et al. Removal of toluene from industrial gas over 13X zeolite supported catalysts by adsorption-plasma catalytic process. J Chem Technol Biotechnol 2017;92:2276–86.
[45] Tao S, Li C, Fan X, Zeng G, Lu P, Zhang X, et al. Activated coke impregnated with cerium chloride used for elemental mercury removal from simulated flue gas. Chem Eng J 2012;210:547–56.
[46] Wang Y, Li C, Zhao L, Xie Y, Zhang X, Zeng G, et al. Study on the removal of elemental mercury from simulated flue gas by $Fe_{(2)}O_{(3)}$-$CeO_{(2)}$/AC at low temperature. Environ Sci Pollut Res Int 2016;23:5099–110.
[47] Artur P. Terzyk, The influence of activated carbon surface chemical composition on the adsorption of acetaminophen (paracetamol) in vitro Part II. TG, FTIR, and XPS analysis of carbons and the temperature dependence of adsorption kinetics at the neutral pH, Colloids and Surfaces A: Physicochemical and Engineering Aspects 2001;177:23–45.
[48] Huang Y, Tang J, Gai L, Gong Y, Guan H, He R, et al. Different approaches for preparing a novel thiol-functionalized graphene oxide/Fe-Mn and its application for aqueous methylmercury removal. Chem Eng J 2017;319:229–39.
[49] Yu D, Liu Y, Wu Z. Low-temperature catalytic oxidation of toluene over mesoporous MnO_x–CeO_2/TiO_2 prepared by sol–gel method. Catal Commun 2010;11:788–91.
[50] Hernández WY, Centeno MA, Ivanova S, Eloy P, Gaigneaux EM, Odriozola JA. Cu-modified cryptomelane oxide as active catalyst for CO oxidation reactions. Applied Catalysis B: Environmetal 2012;123–124:27–35.
[51] Liao Y, Zhang X, Peng R, Zhao M, Ye D. Catalytic properties of manganese oxide polyhedra with hollow and solid morphologies in toluene removal. Appl Surf Sci 2017;405:20–8.
[52] Kim SC, Shim WG. Catalytic combustion of VOCs over a series of manganese oxide catalysts. Appl Catal B: Environ 2010;98:180–5.
[53] Yao J, Zhang P, You H, He Y. Study on performance of cerium mixed into copper oxide loading catalysts in catalytic oxidation of toluene, 25 (2009) 150–154.
[54] Feng J, Hou Z-Y, Zhou X-Y, Zhang H-L, Cheng T-Q, Lin T, et al. Low-temperature catalytic oxidation of toluene over Mn–Co–O/$Ce_{0.65}Zr_{0.35}O_2$ mixed oxide catalysts. Chem Pap 2017;72:161–72.
[55] Liao Y, Fu M, Chen L, Wu J, Huang B, Ye D. Catalytic oxidation of toluene over nanorod-structured Mn–Ce mixed oxides. Catal Today 2013;216:220–8.
[56] Zhang G, Li Z, Zheng H, Fu T, Ju Y, Wang Y. Influence of the surface oxygenated groups of activated carbon on preparation of a nano Cu/AC catalyst and heterogeneous catalysis in the oxidative carbonylation of methanol. Appl Catal B: Environ 2015;179:95–105.
[57] Pozan GS. Effect of support on the catalytic activity of manganese oxide catalyts for toluene combustion. J Hazard Mater 2012;221–222:124–30.
[58] Tang Q, Gong X, Zhao P, Chen Y, Yang Y. Copper–manganese oxide catalysts supported on alumina: Physicochemical features and catalytic performances in the aerobic oxidation of benzyl alcohol. Appl Catal A 2010;389:101–7.
[59] Li L, Jing F, Yan J, Jing J, Chu W. Highly effective self-propagating synthesis of CeO_2 -doped MnO_2 catalysts for toluene catalytic combustion. Catal Today 2017;297:167–72.
[60] Kim SC, Park Y-K, Nah JW. Property of a highly active bimetallic catalyst based on a supported manganese oxide for the complete oxidation of toluene. Powder Technol 2014;266:292–8.
[61] Wang HP, Lu YY, Han YX, Lu CL, Wan HQ, Xu ZY, et al. Property of a highly active bimetallic catalyst based on a supported manganese oxide for the complete oxidation of toluene. Appl Surf Sci 2017;420:260–6.
[62] Zimowska M, Michalik-Zym A, Janik R, Machej T, Gurgul J, Socha RP, et al. Catalytic combustion of toluene over mixed Cu–Mn oxides. Catal Today 2007;119:321–6.
[63] Łamacz A, Krztoń A, Djéga-Mariadassou G. Study on the selective catalytic reduction of NO with toluene over CuO/$CeZrO_2$. A confirmation for the three-function model of HC-SCR using the temperature programmed methods and in situ DRIFTS. Appl Catal B: Environ 2013;142–143:268–77.
[64] Li WB, Wang JX, Gong H. Catalytic combustion of VOCs on non-noble metal catalysts. Catal Today 2009;148:81–7.
[65] Wang Y, Deng W, Wang Y, Guo L, Ishihara T. A comparative study of the catalytic oxidation of chlorobenzene and toluene over Ce-Mn oxides. Mol Catal 2018;459:61–70.
[66] Dong XA, Cui W, Wang H, Li J, Sun Y, Wang H, Zhang Y, Huang H, Dong F. Promoting ring-opening efficiency for suppressing toxic intermediates during photocatalytic toluene degradation via surface oxygen vacancies. Sci Bull 2019;10:669–78.
[67] Zhao B, Yan B, Yao S, Xie Z, Wu Q, Ran R, et al. $LaFe_{0.9}Ni_{0.1}O_3$ perovskite catalyst with enhanced activity and coke-resistance for dry reforming of ethane. J Catal 2018;358:168–78.